Chapter 12

Remote Sensing Retrieval Study of the Surface Kinetic Parameters in the Yangtze Estuary and Its Adjacent Waters

Shengbo Chen and Lihua Wang

Additional information is available at the end of the chapter

http://dx.doi.org/10.5772/intechopen.72461

Abstract

Wind and current are significant parameters in the hydrodynamic processes, making a significant effect on the expansion of the Yangtze (Changjiang River) Diluted Water, sediment transport, resuspension and shelf circulation in the Yangtze Estuary. They are indispensable as input parameters in the numerical simulation of these phenomena. Synthetic aperture radar (SAR) can acquire data with different resolutions (down to 1 m) and coverage (up to 400 km) over a site during day or night time under all weather conditions, being capable of providing ocean surface kinetic parameters with high resolution. SAR images were collected to verify and improve the validity of wind direction retrieval by 2D fast Fourier transformation (FFT) method, wind speed by CMOD4 model and current by Doppler frequency method. These SAR-retrieved wind and current results were analyzed and assessed against in situ data and corresponding numerically simulated surface wind and current fields. Comparisons to the in situ and simulations show that 1) SAR can measure sea surface wind fields with a high resolution at sub-km scales and provide a powerful complement to conventional wind measurement techniques. 2) The Doppler shift anomaly measurements from SAR images are able to capture quantitative surface currents, thus are helpful to reveal the multi-scale upper layer dynamics around the East China Sea.

Keywords: multi-source remote sensing images, sea surface wind, sea surface current, fast Fourier transformation, Doppler frequency

1. Introduction

Sea surface wind and current, directly related to almost all ocean water movement, are one of the most basic and crucial parameters in studies of hydrodynamic, ecological processes

and global climatic change [1, 2], including the expansion of Yangtze (Changjiang River) Diluted Water (CDW) and shelf circulation in the Yangtze Estuary. In the summer, CDW extends to the northeast as a plume. While during winter it clings to the Chinese coast to the southwest in a narrow band. In the estuary, the prevailing monsoon climate results in stronger northerly winds during winter and weaker southerly winds during summer. Wind-driven Ekman transport cause the CDW distribution presenting significant seasonal variation [3, 4]. Therefore, it is indispensable to take the high-resolution ocean surface wind into consideration in the accurate numerical simulation of these phenomena. At present, there is lack of high-resolution in situ wind data in the East China Sea (ECS). Prevailing wind vector products are based on meteorological models and satellite-borne scatterometer (SCAT) measurements with only a resolution of around 25 km [5]. This resolution is insufficient to meet the calculation accuracy of the numerical model. SAR can acquire data with different resolutions (down to 1 m) and coverage (up to 400 km) over a site during day or night time under all weather conditions, being capable of retrieving ocean surface wind vectors with high resolution. The ERS-1 was launched in 1991 by European Space Agency, since then, SAR images have been continuously measuring the various global features and observing the ocean surface, such as ocean surface winds, waves, and currents [6–8]. Despite variations of wind field including direction and speed, SAR images have the capability to reveal high-resolution patterns, which can render possible the exciting prospect of measuring ocean surface wind from space, especially in the coastal regions.

For high resolution (~1 km) surface current measurements, it is highly necessary to have a good regular observing system. From the perspectives of economic, ecological and hydrodynamic, these data are of great importance for assimilation in ocean and shelf circulation models, which is capable of providing sufficient predictions of the continuous changes in the estuaries. At present, there are several techniques/equipment currently employed to observe sea flows, including current meter moorings, acoustic Doppler current profilers, drifters as well as remote sensing methods from satellites and ground based High Frequency Radar systems. Pandian et al. [9] discussed their inherent advantages and disadvantages of these instruments and techniques. Geostrophic currents derived from satellite altimetry [10], are now being used regularly in global and regional circulation models. However, it only has a spatial resolution of 25 km, which is too coarse to apply in the coastal regions. High-resolution imaging SARs have been demonstrated to have the promising capabilities for retrieving surface current estimates with resolution of 2–10 km [11–14]. Two techniques have emerged notably the along-track interferometry SAR (AT-INSAR) requiring a split antenna [13, 15, 16] and the single-antenna SAR based on Doppler method [11]. Chapron et al. [17] pioneered to derive and discuss the slant range radar-detected velocity of the ocean surface roughness from Advanced SAR (ASAR) based on Doppler measurements of moving ocean surfaces, probably caused by the small-scale disturbances such as capillary waves. Moreover, their studies presented that the Doppler centroid anomalies observed by ASAR are of a geophysical properties. The Doppler anomalies are generated by the relative motion between ocean surface and radar platform, which are solely connected to the movement of the sea surface roughness elements. These anomalies can reflect the combined action of wind, waves and

currents. The corresponding SAR images based on the Doppler frequency anomaly methods have been successfully applied to observe the Agulhas Current [12, 14], the Gulf Stream [11], the Norwegian Atlantic Current [18] and coastal current in the Yangtze Estuary. Therefore, SAR will play an increasingly critical role in the quantitative studies of ocean surface flow characteristics. In addition, the development of SAR Doppler technology will provide new opportunities for routinely observing and simulating mesoscale ocean processes and coastal current phenomena.

2. Methods

2.1. Sea surface wind

For sea surface wind direction extraction, 2D fast Fourier transformation (FFT) in the spectral domain was employed. The processing steps were as follows in order to obtain high-resolution wind direction information. Firstly, all pixels in SAR images not affected by the local ocean surface wind, such as land, surface slicks, ships and artifacts, were masked. Secondly, SAR images were divided into sub-images, which was set to 6.4 × 6.4 km to quantitatively express the resolution of wind direction. The reason for setting this scale is that the wind-driven streak characterizes typically present km-scale spacing. Next, we used the 2D FFT in SAR scenes to obtain the Fourier spectra and filters to eliminate high-frequency speckle in Fourier spectra. Fourthly, we constructed the regression according to the least-squares estimation, and set the energy densities for wavelengths between 500 and 2000 m. At last, the orientation of the wind streaks with an 180° directional ambiguity was extracted, which is perpendicular to the regression line. The directional ambiguity was subsequently removed according to the QuikSCAT or ECMWF wind products.

For sea surface wind speed extraction, the GMF CMOD4 was employed here. And it was originally designed to derive wind speed from SCAT, the SCAT instruments operate at C-band with VV polarization. SAR also operate at the same wavelength, therefore, the GMF CMOD4 is suitable for SAR images with VV polarization. The relationship between wind speed, wind direction, and NRCS (the GMF) is generally expressed by the form (1) [19]

$$\sigma^0 = A(u_{10}, \theta)\left[1 + b(u_{10}, \theta)\cos\phi + c(u_{10}, \theta)\cos\varphi\right]^B \quad (1)$$

where σ^0 is the NRCS in linear units; ϕ is the wind direction versus antenna look direction; u_{10} is wind speed; θ is nadir incident angle; and A, b, c, and B are model parameters depending on radar frequency, polarization, u_{10}, and θ.

The GMF CMOD4 employed here was developed and validated using a large amount of measured data. For the C-band SAR images with HH polarization, a hybrid model including CMOD4 and the polarization ratio [20, 21] were employed. A flowchart of sea surface wind retrieval scheme is shown in **Figure 1**.

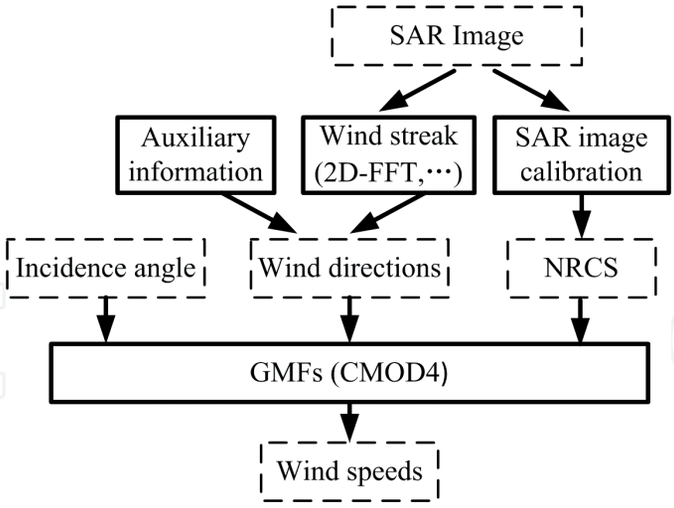

Figure 1. Flowchart of wind retrieval from SAR image.

2.2. Sea surface current

In the processing of SAR images, the Doppler centroid frequency of the SAR signal f_{DC} is an important input parameter to obtain high resolution SAR images. For ASAR WSM scene in the range direction, a systematic grid of Doppler centroid frequencies has 100 pixels, while in the azimuth direction it contains a given number, which is dependent on the scene coverage. The cross-track pixel spacing is about 3.5 km in the far range direction and 9 km in the near range direction, while in the azimuth direction it is about 8 km (1) [22–25].

The velocity of satellite along track relative to the rotating Earth results in a frequency motion f_{DP}. Using CFI software complied in C language, the parameters of f_{DP} and footprint geolocation can be precisely computed at any look angle and any orbit time [23, 25].

There are several influence factors contaminating the geophysical Doppler frequency shift information, including radial discontinuities, antenna mis-pointing, strong discrete targets, low signal-to-noise ratio areas and Doppler estimator bias. Therefore, the estimation errors f_{err} must be removed first [11, 12, 22–24]. The scenes with enough land pixels for each range line number from the adjacent orbits/acquisition time were applied as reference image to eliminate the Doppler anomaly biases relying on elevation angle (**Figure 2**). Hansen et al. [23] introduced the details of Doppler centroid anomaly.

Wind-induced streaks are presented in the ASAR images. So, 2D FFT can be employed to extract the wind direction and CMOD4 to calculate the wind speed. Based on the CDOP model [24], we applied the ASAR derived-wind vectors to yield an estimation of the wind contributions to the Doppler frequency. In turn, these Doppler contributions from wind induced f_w were then removed.

The geophysical Doppler anomaly f_g can be calculated using the following Eq. (2) and can be converted with Eq. (3) to the surface current fields [23, 25] (2)

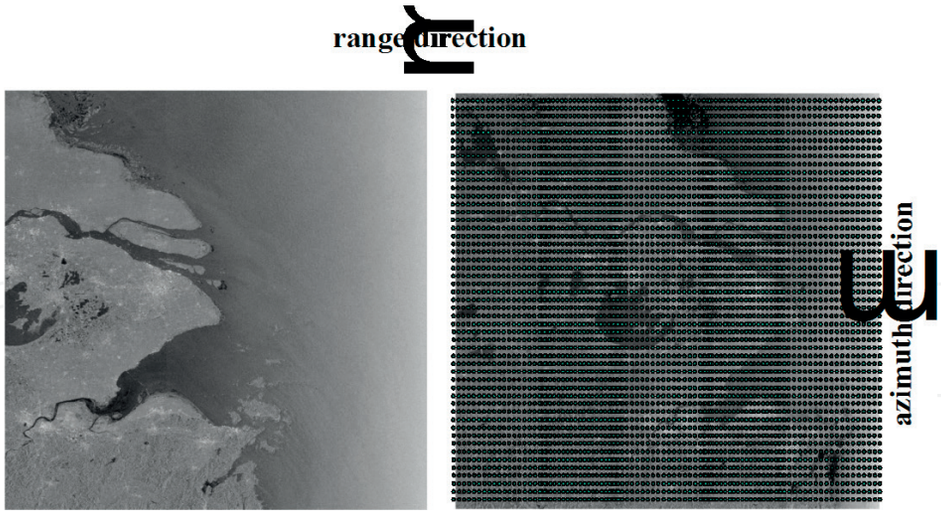

Figure 2. The NRCS of ASAR WSM scene over Yangtze estuary on 31 January 2005 (left) and 5 February 2005 (right). Superimposed points on the right plot are the Doppler centroid grids. Arrows denote azimuth and range directions of ASAR image.

$$f_g = f_{DC} - f_{DP} - f_{err} - f_w \tag{2}$$

$$V = -\pi f g / k e \sin\theta \tag{3}$$

where k_e is 112 m^{-1} for the radar wavelength of 5.6 cm of the Envisat ASAR instrument and θ denotes radar incidence angle.

3. Results and discussion

3.1. SAR-retrieved wind fields

Figure 3a and **b** showed the estimated wind directions by 2D FFT in the spectral domain at the Dajishan and Tanhu meteorological stations. Since the wind shadowing are visible in the SAR image, we can directly remove the 180° directional ambiguities. The sea surface wind directions retrieved from SAR scene are approximate to the observed measurements, which were presented in **Table 1**. Results from SAR scene and by WRF model are generally in good agreement with the observed values. Particularly, the difference between the SAR-retrieved wind direction and the observed measurement is less than 5°. When comparing wind speed retrieved from SAR scene and the WRF model with observed data, the results showed both retrieved wind speed are a little lower than the observed data. Generally, wind direction and wind speed derived from the SAR data are slightly better than the WRF model outputs.

Two ERS-2 SAR images obtained over the Yangtze coastal area on 4 May 2006 were mosaicked and presented in **Figure 3c**. The upper SAR data were captured at 02:27 UTC and lower at

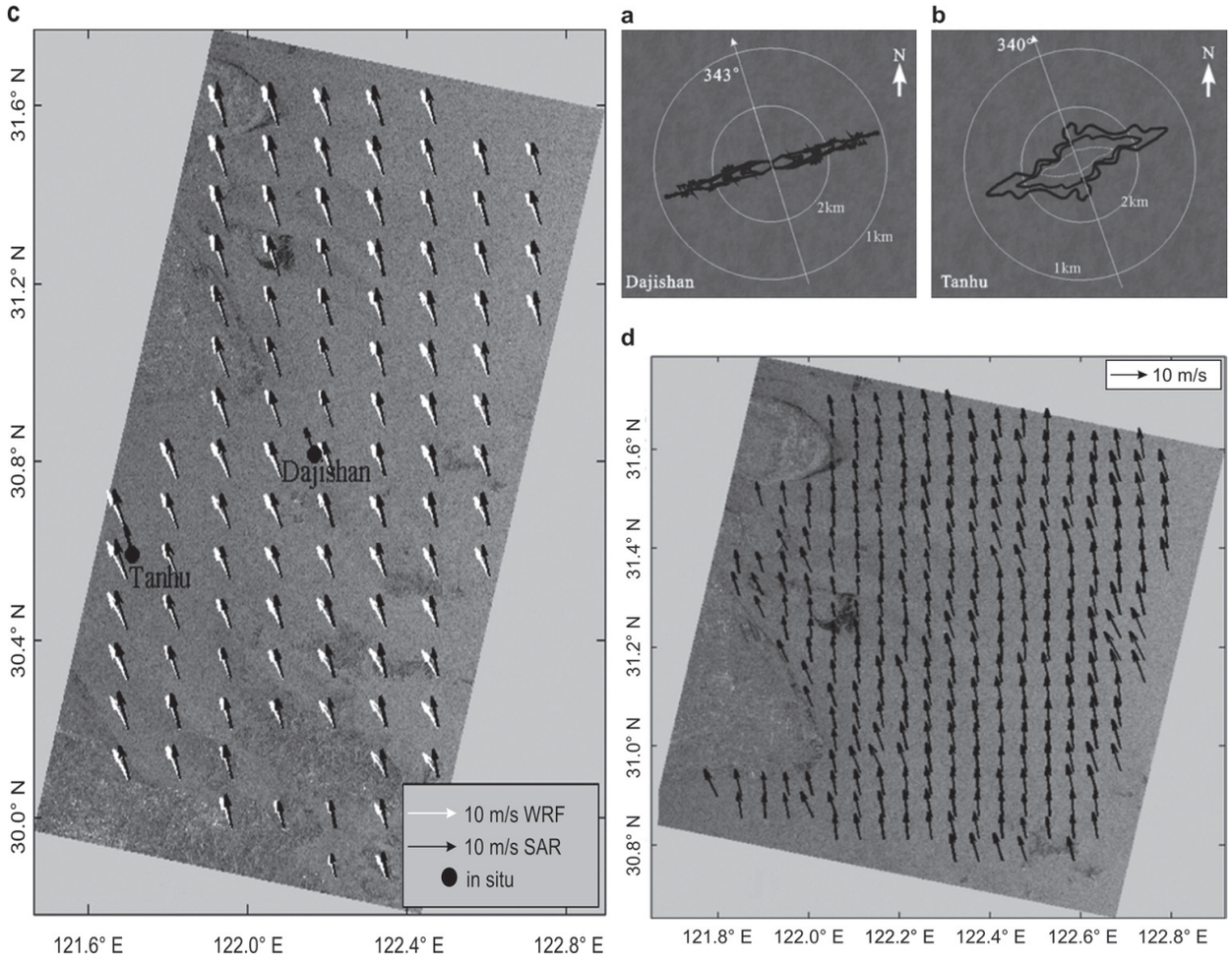

Figure 3. Low-wavenumber of sea surface wind direction at (a) Dajishan and (b) Tanhu; wind vectors (c) from two ERS-2 SAR scenes on 4 May 2006, and (d) 5 km resolution wind field from SAR image.

Test site	Wind direction (°)			Wind speed (m/s)		
	Observed data	SAR-retrieved	WRF model	Observed data	SAR-retrieved	WRF model
Dajishan	340	343.0	335.0	9.8	8.6	8.3
Tanhu	345	340.0	329.6	10.3	9.9	9.5

Table 1. Extracted wind field results and observed wind vectors.

02:28 UTC, respectively. The wind vector results were superimposed on the SAR images. The black arrows denoted the wind retrieved from SAR images and the white arrows presented those calculated by WRF model. The observed data at the Dajishan and Tanhu meteorological stations were also superimposed. Since the wind from WRF model are available on a 1-h basis, we interpolated the wind vectors into the precise SAR acquisition time using the natural neighbor method. According to **Figure 3c**, roughly speaking, both in wind direction and magnitude, the vectors derived from SAR are in good agreement with the outputs by the WRF model.

An ERS-2 SAR imaged on 4 May 2006, at 02:27 UTC, covering the Yangtze and adjacent area was shown in **Figure 3d**. Wind vectors with a resolution of 5 km were superimposed on the SAR image. According to the wind shadowing visible in SAR image, the 180 degree wind direction ambiguities were removed. The wind direction in **Figure 3d** was closely analogous to that on the coarse grid of the WRF model (the upper part of **Figure 3c**). While close to the coastal area of Yangtze Estuary, the wind direction was slightly changed westward, however, it was not effectively simulated by the WRF model. In the upper part of **Figure 3c**, wind speed derived from SAR image was very close to the outputs from the WRF model.

Figure 4a and **b** showed the scatterplots of QuikSCAT products vs. SAR results. From these robust results, we could find that both QuikSCAT and SAR images are valid data sources to obtain sea surface wind fields. QuikSCAT is still best suitable for open ocean measurements due to its larger coverage, although it can only yield wind fields with resolution up to 12.5 km. However, wind fields can remarkably change over a few km, even over a smaller scale in the coastal areas. SAR images with high resolution (up to 1 m) are capable of producing sub-km resolution wind vectors. Therefore, an improved global wind product can be obtained by combining QuikSCAT wind products in open ocean areas with SAR-derived wind fields in coastal areas.

The wind scatterplots of WRF vs. SAR were plotted in **Figure 4c** and **d**. The results suggested that wind fields computed by WRF and extracted by SAR do not correspond as closely as those between SAR and QuikSCAT. Furthermore, when CMOD4 adopted to extract wind speeds from SAR images, it would lead to underestimation in high wind speeds larger than 20 m/s and overestimation in small speeds lower than 3 m/s (**Figure 4d**).

From **Table 1** and **Figure 3c**, we could find that wind directions retrieved from SAR images are in good agreement with the observed data at the Tanhu and Dajishan. Specifically, the discrepancies are less than 5°. These promising results may be explained as follows. The algorithm for wind direction extraction based on 2D FFT was improved by finding average position of the first three maximum spectral value instead of applying the position of single spectrum peak. This process was helpful to enhance the stability of the wind direction information extraction. In addition, wind direction from SAR image based on 2D FFT method is dependent on the orientation of typical km-scale surface features. When atmospheric conditions are relatively steady or sea surface wind speed is very small, precise wind directions would become difficult to derive. The wind speed of the example SAR image is large, about 8–10 m/s. Therefore, it can be deduced that wind direction can be precisely extracted by 2D FFT method from SAR images when wind speed is larger than about 7–8 m/s. On the other hand, large wind direction discrepancies between SAR-retrieved and in situ observations are probably due to non-wind-driven features imaged in SAR scene at the same scale as wind-driven. These features are not related with the ocean surface wind direction, e.g., ocean waves.

Along the coast of Yangtze Estuary, the SAR-retrieved wind vector results presented larger variability in direction and much better detail information in structure than the WRF outputs (**Figure 3d**). This is dependent on the high spatial resolution of SAR snapshot imaging a highly turbulent wind field, while relatively low resolution of the WRF numerical model cannot capture such small-scale signals. Moreover, there are several factors may result in the

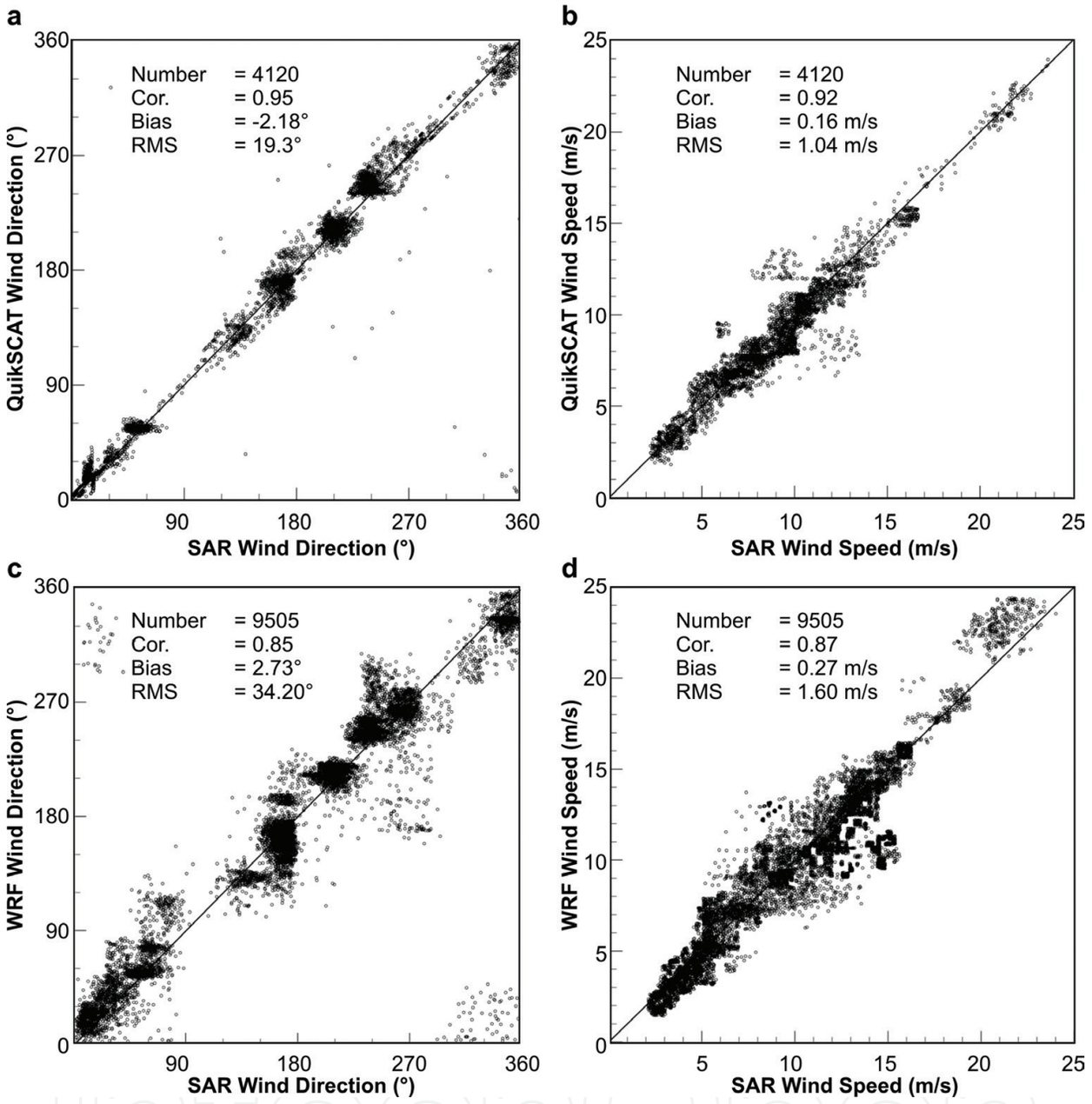

Figure 4. Scatterplots of wind results from QuikSCAT vs. SAR and WRF vs. SAR.

spatial inhomogeneity in the wind field. In the Yangtze Estuary, the variable topography is one of the factor. The improved SAR wind retrieval method in this study indeed resolve spatial inhomogeneity of the variable sea surface wind vector.

A linear regression of sea surface wind direction retrieved from SAR images and QuikSCAT wind direction presented a bias of −2.18° and root mean square error of 19.3°. These results are better than those between SAR measurements and WRF outputs, whose values are 2.73° and 34.20°, respectively. The ECS is located in a subtropical monsoon climate area. SAR images can effectively capture the homogeneous distribution of wind. Therefore, the 2D FFT method in the spectral domain is well suitable for extracting wind direction in the ECS. The correlation

coefficient R^2 in the case-by-case comparisons of SAR-retrieved wind direction with QuikSCAT and WRF results are 0.95 and 0.82, respectively. The high R^2 values indicated the improved 2D FFT method used to deduce wind direction is reliable. The wind speed linear regression analysis between SAR images and QuikSCAT has a bias of 0.16 m/s and root mean square error of 1.04 m/s. These results are slightly better than those for the linear analysis of wind speeds from SAR and WRF model, whose values are 0.27 m/s and 1.60 m/s, respectively. The comparisons of SAR wind speeds with QuikSCAT products showed high R^2 value of 0.92, which approaches to the $R^2 = 0.93$ manifested by Monaldo et al. [26].

Therefore, for C-band SAR images with VV polarization, the algorithm based on 2D FFT extracting sea surface wind direction and the CMOD4 model computing wind speed are prominent and promising to obtain sea surface wind field. Especially in the coastal areas, the large spatial coverage and multi-resolution (especially high resolution) of SAR scene, with its all day, all weather capability, makes it indispensable in the observation of detailed sea surface kinetic parameters and features.

3.2. SAR-retrieved current fields

Figures 5 and **6** showed f_{DC}, f_{DP}, the raw Doppler anomaly and the geophysical Doppler frequency anomaly f_g from ASAR WSM scene on 31 January 2005 and 5 February 2005, respectively. There were large variability of the raw Doppler centroid anomaly over interaction zone between land and sea, even over land areas (**Figure 5c** and **6c**). However, the Doppler frequency anomaly should be zero over land since it is immobile relative to the Earth. Along the azimuth direction, the strong backscatter signal gradient is one of the main sources of Doppler frequency bias, which is particularly exhibited over the coastline areas. In addition, the erroneous Doppler frequencies in the range direction are obvious as vertical stripes of increased or decreased Doppler anomalies, and present at the transition area between different sub-swaths. The biases are also from artifacts. The error correction were therefore proceeded both in the azimuth and range directions. The root mean square offset over land was reduced by 13.7 and 12.1 Hz that was from 24.5, 21.4 Hz of the raw Doppler anomaly to 10.8, 9.3 Hz (**Table 2**). And it was further reduced to 6.2, 6.1 Hz, respectively (**Table 2**) after removing the outlying values. The geophysical Doppler anomaly after removal of the wind-induced Doppler frequency were shown in **Figures 5d** and **6d**. Surface current fields according to the Eq. (3) were calculated and presented in **Figure 7a** and **b**, respectively. The SAR Doppler method produced Doppler velocity with a resolution about 8 km in azimuth direction and 4 km in range direction. The negative range Doppler velocity values correspond to the sea surface velocities towards the sensor platform, whereas positive values suggest a current away from the platform.

In **Figure 7a** of surface Doppler velocities from ASAR WSM scene on 31 January 2005, there is a distinct directional change located at about 31.5°N. In the Hangzhou Bay area, a southeasterly current is encountered. At the time of image acquisition, the wind streak was clearly visible on the SAR scene and exhibited a qualitative correlation with the SAR backscatter signal. 2D FFT and CMOD4 model were adopted to extract the wind direction and wind speed information, respectively. Results showed that the northwesterly wind increased from

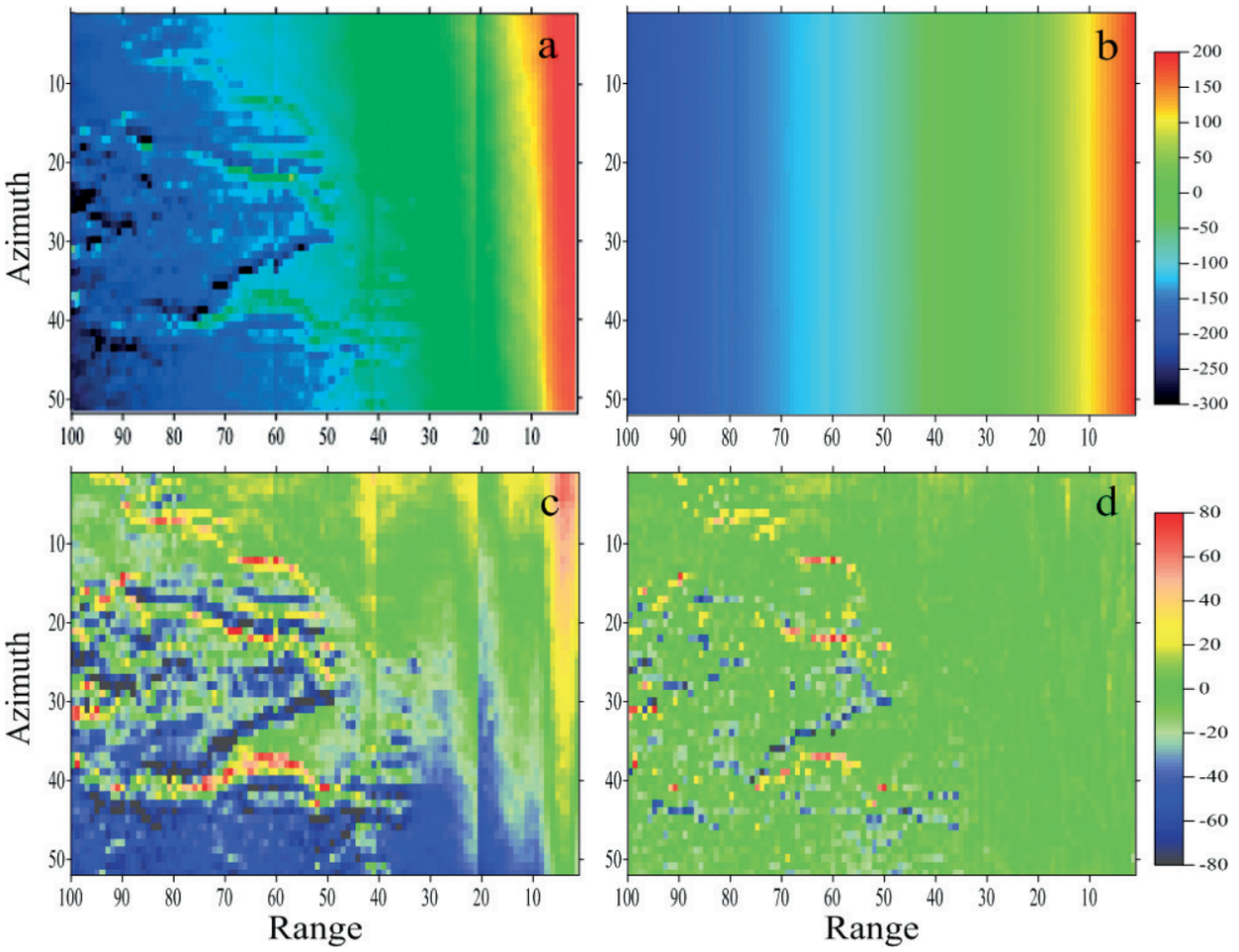

Figure 5. The Doppler centroid grid of ASAR WSM scene on 31 January 2005. (a) f_{DC}. (b) f_{DP}. (c) the raw Doppler centroid anomaly and (d) f_g.

8 to 11 m/s with the distance from the shoreline. At the Tanhushan meteorological station, it is particularly the case at low tide, so the tidal current should be relatively low. However, the range Doppler velocity here is relatively large in **Figure 7a**. This was probably related to the underwater topography and the combination action of the ocean wind, wave and current.

In **Figure 7b** of the range Doppler velocity on 5 February 2005, the Doppler currents located from 122.5°E to west range from −1.2 to −0.2 m/s. This corresponds with a westerly/southwesterly sea surface current. In the area located from 122.5°E to east, the range Doppler currents are mostly positive, corresponding an easterly/northeasterly surface current. Negative strong Doppler velocity occur in the Hangzhou Bay areas. At the scene acquisition time, wind directions retrieved by 2D FFT method are from the northeast, i.e. towards the radar sensor. Wind speeds calculated by CMOD4 model are between 9 and 11 m/s. At the Tanhushan station, Doppler velocity is −0.25 m/s at 40 minutes after high tide. At the remaining four tidal stations, the Doppler velocities were very variable even if they all located at about 2–3 h after high tide. Therefore, we could deduce that any Doppler velocity map such as **Figure 6a** and **b** represent the wind, wave and current patterns in a rather complicated way. Local variables in the wind, wave field and underwater topography would exacerbate the interpretation of geophysical Doppler velocity.

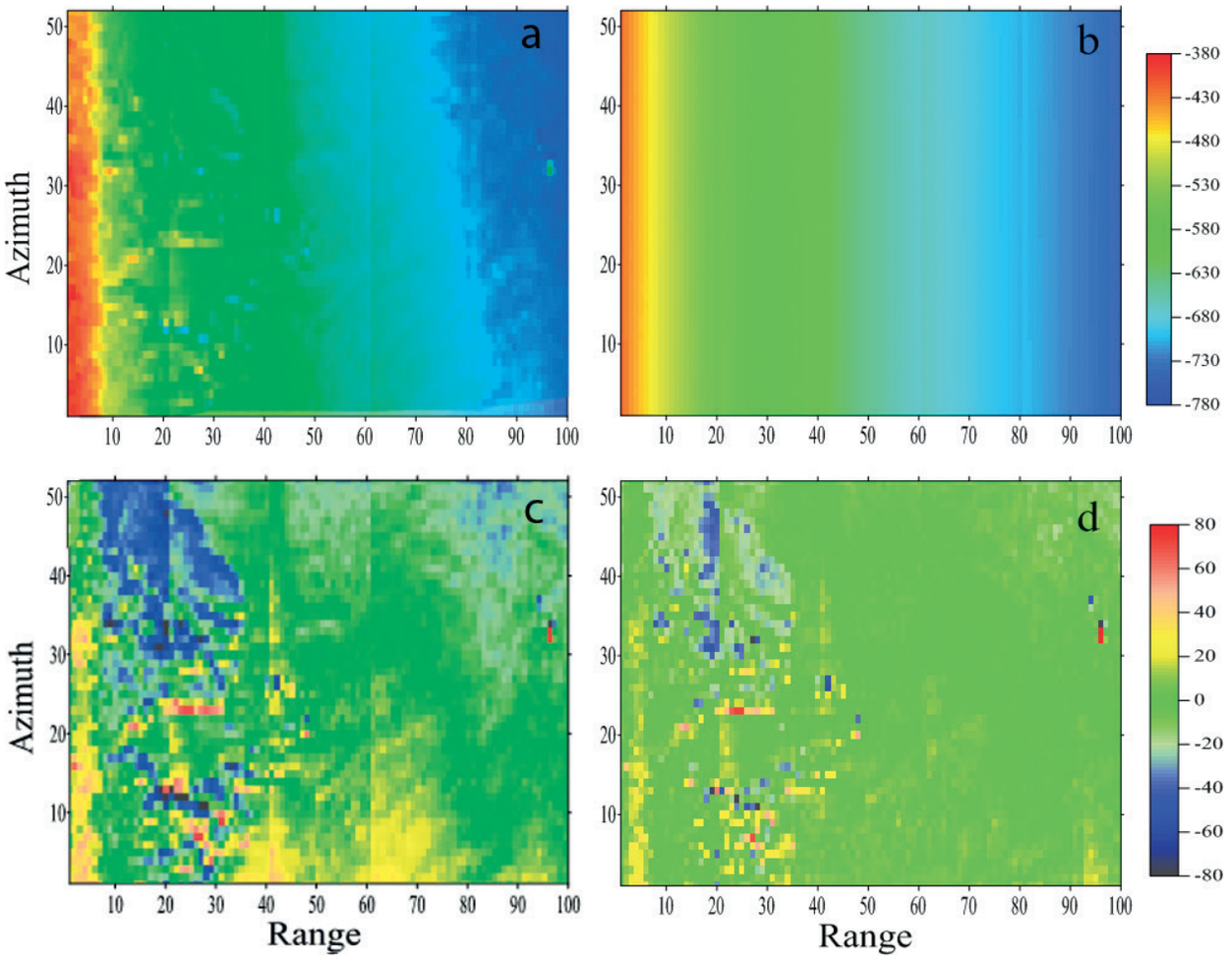

Figure 6. The Doppler centroid grid of ASAR WSM scene on 5 February 2005. (a) f_{DC}. (b) f_{DP}. (c) the raw Doppler centroid anomaly and (d) f_g.

Acquisition time of ASAR scene	RMS of Doppler anomaly/Hz			
	raw	After azimuthal correction	After bias correction	After outliers removal
31 January 2005	24.5	19.0	10.8	6.2
05 February 2005	21.4	16.1	9.3	6.1

Table 2. Doppler centroid anomaly bias over land of the scenes.

The estimated Doppler velocity fields in the above two images showed that the strongest Doppler velocities appeared in the Hangzhou Bay area, where the velocities are up to 0.8–1.0 m/s. These high current values are mainly influenced by the interaction of wind, wave and tide. As the two cases at spring tide, the retrieved Doppler velocities represent the relatively intense currents. The ability of SAR image to extract strong surface currents based on the Doppler frequency method was also shown in the Agulhas Return Current area [14]. However, large Doppler velocities are usually related to strong NRCS gradients in the SAR signal. Accordingly, the strong NRCS would lead to the overestimation of Doppler velocity. Therefore, the error correction of Doppler shift in azimuth direction must be sufficient, if not,

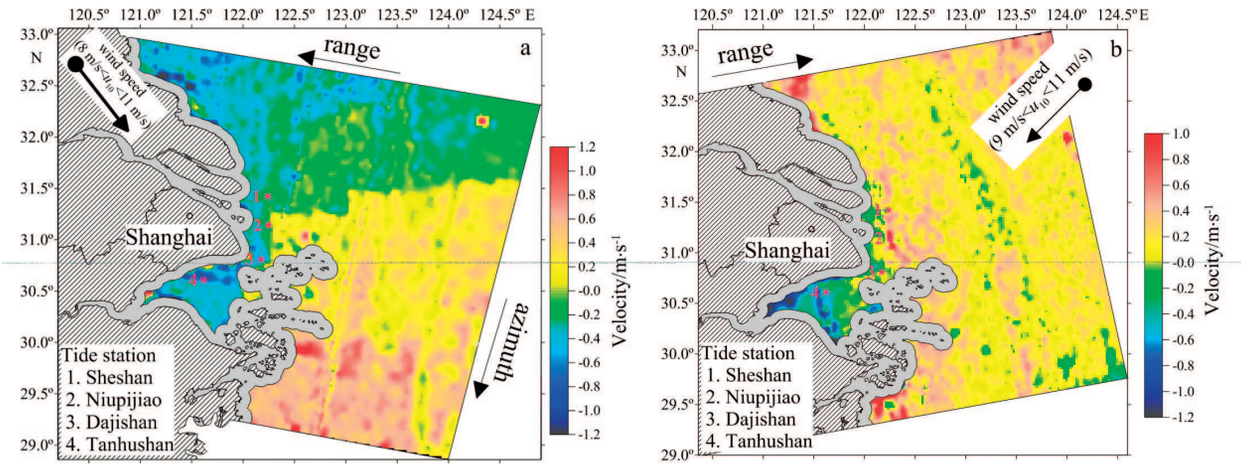

Figure 7. Surface range Doppler velocities from WSM images (a) on 31 January 2005 and (b) on 5 February 2005. The color scale is given in unit of m/s.

it will make a negatively effect on Doppler velocity estimation. In addition, more attention and analysis should be taken in the region near the land-sea boundaries.

The SAR imaging geometry with regard to the sea surface current field derived from Doppler method is highly significant to the Doppler velocity quality. In the Yangtze Estuary, the flow is along a southeast/northwest axis. Since the ENVISAT ASAR is right-looking imaging radar, the descending track configuration is well suitable for capturing spatial variations of current field. Moreover, the descending track SAR image the Yangtze Estuary mouth at the high radar incidence angle (**Figure 7a**), which is helpful to reduce the retrieval error from the effect of incidence angle.

For the Doppler centroid anomaly method, in order to examine and assess its capability for retrieving surface current from SAR images, we compared the Doppler current, both from SAR ascending and descending pass, with FVCOM outputs. In general, both in magnitude and directions, they exhibited the similar surface current field features (**Figure 8a** and **b**). For quantitative comparison, we extracted two transects from ASAR results and FVCOM surface flow maps (**Figure 8a** and **b**), one at about 30.5°N latitude on ASAR descending pass, the other at about 30.7°N latitude on ASAR ascending image.

In both transects, surface current directions derived from ASAR images and simulated by FVCOM are in good agreement (**Figure 8c** and **d**). As a whole, the comparison of velocity is also robust provided the different speed is within +/−0.2 m/s. For the surface current velocities retrieved from the ASAR, the maximum values in both cases are up to1.0 m/s, whereas the maximal velocity simulated by FVCOM is only 0.6 m/s on 5 February 2005 and 0.8 m/s on 31 January 2005. The maximum discrepancy is 0.35 m/s located at about 121.2° E on 5 February 2005, and 0.42 m/s at 122.7°E on 31 January 2005. The corresponding incidence angle is 24.0° and 27.5°, respectively, which are both below 30°. We further computed the average velocity difference below and above 30° radar incidence angle, between Doppler velocities and FVCOM outputs. The results showed that above 30° radar incidence angle, the difference was only 0.09 m/s on 31 January 2005 and 0.10 m/s on 5 February 2005, i.e., the difference could be

http://dx.doi.org/10.5772/intechopen.72461

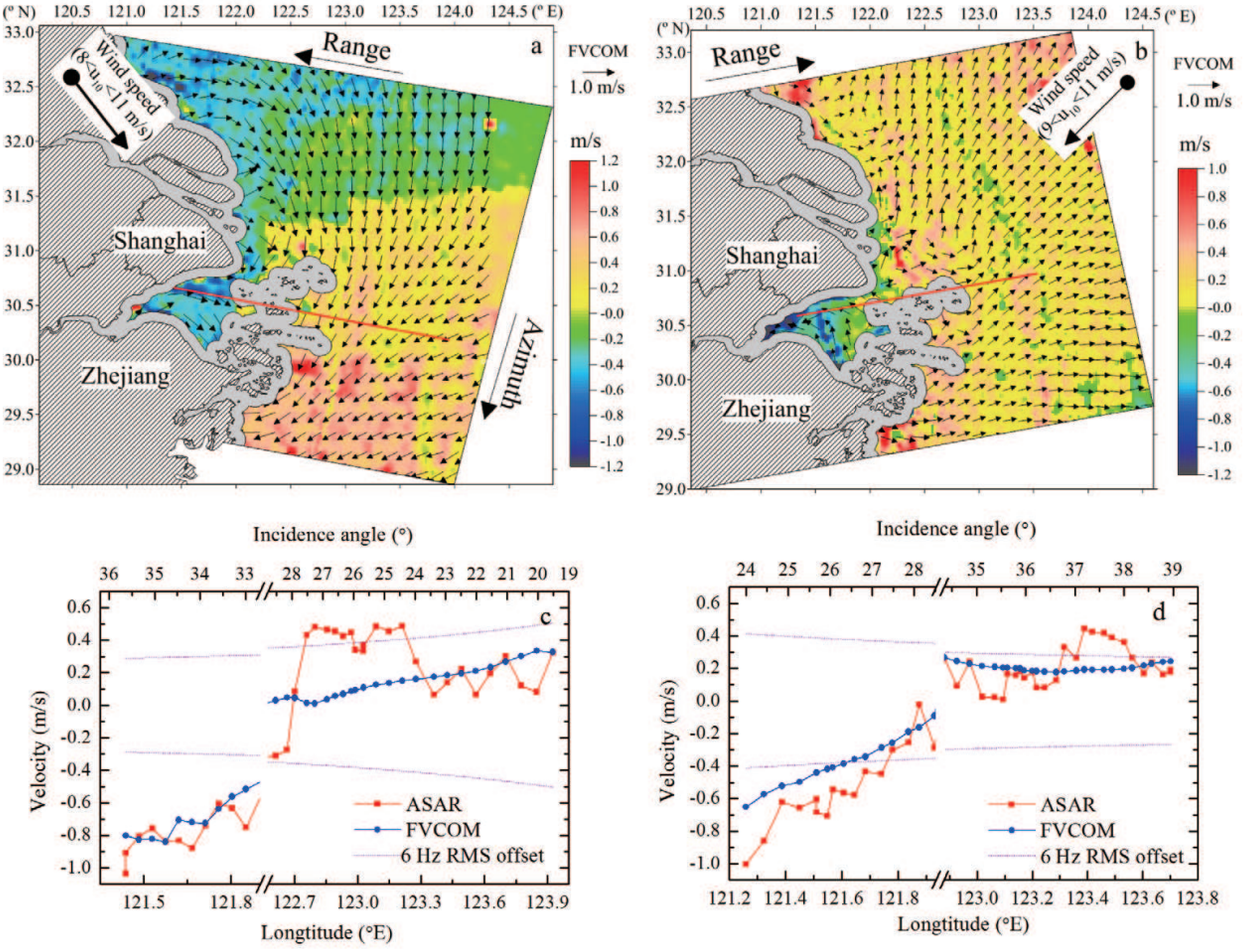

Figure 8. ASAR Doppler velocity (a) on 31 January 2005 and (b) on 5 February 2005. Superimposed were the FVCOM surface currents as arrows. The color scale is given in unit of m/s. Transects of ASAR Doppler and FVCOM velocities (c) on 31 January 2005 and (d) on 5 February 2005.

ignored if taking the retrieval error into the consideration. Whereas, the difference increased to 0.24 m/s on 31 January 2005 and 0.18 m/s on 5 February 2005 below 30° radar incidence angle. These results were well matched with the previous studies [11, 12, 27] and further corroborated and revealed a considerable increase in the ASAR Doppler velocity error below 30° radar incidence angle.

The dominant current direction of FVCOM result on 31 January 2005 is southerly-southwesterly (**Figure 8a**) from 122.2°E to east. The ASAR-retrieved current only capture the surface current velocity in the range direction, i.e. westerly-northwesterly or easterly-southeasterly. Therefore, the Doppler range Doppler velocities are rather weak, below +/− 0.15 m/s in the area from 31.0°N to north. On the contrary, the current direction simulated by FVCOM on 5 February 2005 (**Figure 8b**), principally presented motions easterly and northeasterly from 122.5°E to east. This direction corresponds well with the slant range direction of ASAR, i.e. the line of sight direction, at least at south of about 31.5°N. Therefore, the retrieval of surface range Doppler current on 5 February 2005 is more accurate and yields a better measurement of the real local sea surface current.

Although the range Doppler velocity results involve spatial change, an obvious correlation exhibits between FVCOM outputs and ASAR Doppler velocities in Yangtze Estuary. The correlation coefficient is 0.56 for the 31 January 2005 case and 0.59 for the 5 February case. In consistence with the previous studies [12, 14, 18], the accuracy of range Doppler velocity fields are affected by the radar parameters, including radar wavelength, polarization, incidence angle and antenna information. Nevertheless, the surface current retrieval based on the Doppler frequency anomaly method is undoubtedly helpful to obtain mesoscale ocean dynamics and definitely reveal sea surface features combined with local environmental changes.

The geophysical Doppler anomaly can be obtained from the ASAR WSM scenes using Doppler centroid grid, due to the precise attitude of the ASAR platform [11]. Yet, biases negatively affect the Doppler centroid frequency, subsequently affect the retrieval accuracy of the range Doppler velocity. Therefore, for the extraction of accurate range Doppler surface velocity estimation, in turn, the more real surface current, error corrections and bias removal are extremely required.

The comparison and validation of ASAR-retrieved Doppler current against the flow simulated by FVCOM showed promising results in both direction and magnitude. Therefore, the Doppler frequency method is capable of extracting innovative measurement of surface current at Yangtze Estuary. These range Doppler velocities from ASAR scenes based on Doppler frequency method are valuable because they can capture and render the multi-scale ocean dynamics around the East China Sea. In addition, the SAR Doppler velocities possess the capability to yield sufficiently and precisely spatial information for validation of high resolution ocean and coastal simulation models in the near future. Further processing and analyzing SAR scenes, together with in situ measurement at the Yangtze Estuary, will undoubtedly promote and implement routine observation of multi-scale sea surface dynamic.

Author details

Shengbo Chen[1] and Lihua Wang[2]*

*Address all correspondence to: wanglh@cuit.edu.cn

1 College of Geo-exploration Science and Technology, Jilin University, Changchun, China

2 College of Resources and Environment, Chengdu University of Information Technology, Chengdu, China

References

[1] Blanton J, Wenner E, Werner F, Knott D. Effects of wind-generated coastal currents on the transport of blue crab megalopae on a shallow continental shelf. Bulletin of Marine Science. 1995;**57**(3):739-752

[2] Genovese SJ, Witman JD. Wind-mediated diel variation in flow speed in a Jamaican back reef environment: Effects on ecological processes. Bulletin of Marine Science. 2004; **75**(2):281-293

[3] Zhu JR, Li YP, Shen HT. Numerical simulation of the wind field's impact on the expansion of the Changjiang River diluted water in summer. Oceanologia et Limnologia Sinica. 1997;**28**(1):72-79 (in Chinese with English abstract)

[4] Chang PH, Isobe A. A numerical study on the Changjiang diluted water in the yellow and East China seas. Journal of Geophysical Research. 2003;**108**(C9):1-17. DOI: 10.1029/2002JC001749

[5] Horstmann J, Koch W, Lehner S, Tonboe R. Wind retrieval over the ocean using synthetic aperture radar with C-band HH polarization. IEEE Transactions on Geoscience and Remote Sensing. 2000;**38**(5):2122-2131

[6] Johannessen JA. Coastal observing systems: The role of synthetic aperture radar. Johns Hopkins APL Technical Digest. 2000;**21**:7-14

[7] Fichaux N, Ranchin T. Combined extraction of high spatial resolution wind speed and wind direction from SAR images: A new approach using wavelet transform. Can. J. Remote Sensing. 2002;**28**(3):510-516

[8] Christiansen MB, Koch W, Horstmann J, Hasager CB, Nielsen M. Wind resource assessment from C-band SAR. Remote Sensing of Environment. 2006;**105**(1):68-81

[9] Pandian PK, Emmanuel O, Ruscoe JP, et al. An overview of recent technologies on wave and current measurement in coastal and marine applications. Journal of Oceanography and Marine Science. 2010;**1**(1):1-10

[10] Kerbaol V, Collard F. SAR-derived coastal and marine applications: From research to operational products. IEEE Journal of Oceanic Engineering. 2005;**30**(3):472-486

[11] Chapron B, Collard F, Ardhuin F. Direct measurements of ocean surface velocity from space: Interpretation and validation. Journal of Geophysical Research. 2005;**110**:C07008

[12] Johannessen JA, Chapron B, Collard F, et al. Direct ocean surface velocity measurements from space: Improved quantitative interpretation of Envisat ASAR observations. Geophysical Research Letter. 2008;**35**:L22608

[13] Romeiser R, Thompson DR. Numerical study on the along-track interferometric radar imaging mechanism of oceanic surface currents. IEEE Transactions on Geoscience and Remote Sensing. 2000;**38**(1):446-458

[14] Rouault MJ, Mouche A, Collard F, et al. Mapping the Agulhas current from space: An assessment of ASAR surface current velocities. Journal of Geophysical Research. 2010;**115**:C10026

[15] Romeiser R, Suchand S, Runge H, et al. First analysis of TerraSAR-X along-track InSAR-derived current fields. IEEE Transactions on Geoscience and Remote Sensing. 2010;**48**(2):820-829

[16] Thompson DR, Jensen JR. Synthetic-aperture radar interferometry applied to ship-generated internal waves in the 1989 loch Linnhe experiment. Journal of Geophysical Research Oceans. 1993;**98**(C6):10259-10269

[17] Chapron B, Collard F, Kerbaol V. Satellite synthetic aperture radar sea surface Doppler measurements. Proceedings of the 2nd Workshop Coastal and Marine Applications Synthetic Aperture Radar (SAR). Svalbard, Norway: ESA; 2004

[18] Hansen MW, Johannessen JA, Dagestad KF, et al. Monitoring the surface inflow of Atlantic water to the Norwegian Sea using Envisat ASAR. Journal of Geophysical Research. 2011;**116**:C12008

[19] Stoffelen A, Anderson D. Scatterometer data interpretation: Estimation and validation of the transfer function CMOD4[J]. Journal of Geophysical Research: Oceans. 1997; **102**(C3):5767-5780

[20] Elfouhaily T, Thompson DR, Vandemark D, Chapron BA. New bistatic model for electromagnetic scattering from perfectly conducting random surfaces. Waves in Random Media. 1999;**9**(3):281-294

[21] Thompson DR, Elfouhaily TM, Chapron B. Polarization ratio for microwave backscattering from the ocean surface at low to moderate incidence angles. Geoscience and Remote Sensing (IGARSS), IEEE International Symposium Proceedings. 1999;**3**:1671-1673

[22] Dagestad KF, Hansen MW, Johannessen JA, et al. Inverting consistent surface current fields from SAR. Frascati, Roma: European Space Research Institute; 2010

[23] Hansen MW, Collard F, Dagestad KF, et al. Retrieval of sea surface range velocities from Envisat ASAR Doppler centroid measurements. IEEE Transactions on Geoscience and Remote Sensing. 2011;**49**(10):3582-3592

[24] Mouche A, Dagestad KF, Collard F, et al. On the use of Doppler shift for sea surface wind retrieval from SAR. IEEE Transactions on Geoscience and Remote Sensing. 2012; **50**(7):2901-2909

[25] Wang L, Zhou Y, Ge J, et al. Mapping sea surface velocities in the Changjiang coastal zone with advanced synthetic aperture radar[J]. Acta Oceanologica Sinica. 2014;**33**(11):141-149

[26] Monaldo FM, Thompson DR, Pichel WG, Clemente-Colon PA. Systematic comparison of QuikSCAT and SAR ocean surface wind speeds. IEEE Transactions on Geoscience and Remote Sensing. 2004;**42**(2):283-291

[27] Collard F, Mouche A, Chapron B, Danilo C, et al. Routine high resolution observation of selected major surface currents from space. Proceedings of the Conference of SEASAR. Frascati, Italy: ESA; 2008